

Experimental study of double diffusive gravity currents under rotation

Marshall Ward

1 Introduction

It is well known that when light and heavy fluid are adjacent to each other, there is an unbalanced pressure gradient that triggers an adjustment process towards equilibrium, so that the light fluid finds its way atop the heavy fluid. This dam-break or lock-exchange problem has been analyzed in great detail for laminar flow (e.g. [1]), though the turbulent situation is perhaps not nearly as well understood. But in either case it is clear that, during adjustment, the light fluid will be pushed upward, with the heavy fluid similarly pushed downward, in the form of a hydraulically-forced gravity current. The process, however, becomes more elaborate when the lateral density gradients vary over long lengthscales. Nearly all large-scale terrestrial phenomena, from river outflow to large-scale oceanic gyres, feel the influence of the Earth's rotation, and this drastically alters the adjustment process. To complicate matters even further, the presence of both heat and salinity distributions in the oceans can lead to buoyantly stable density profiles that are nonetheless double diffusively unstable, and is most prevalent when foreign water intrudes as a gravity current into another part of the ocean. Two potential examples of this are the Mediterranean outflow into the North Atlantic and the various boundary currents of the Arctic Ocean, both of which are intrusions of warm salty water into a cold, fresher background; such intrusions also tend to be steered by the topography for some distance. To estimate the role of these intrusions accurately, it is necessary to understand the underlying processes and how they can interact to influence gravity current formation and propagation.

One of the earliest complete analyses of nonrotating gravity currents is due to Benjamin [2]. A major result of his study is that a frictionless gravity current, once established, will propagate at a constant speed of $c = \sqrt{2g'h_b}$, where g' is the reduced gravity and h_b is the lower fluid depth. It was also shown that, far upstream of the front, the thickness of the lower fluid will occupy only half of the total depth. If friction is introduced, the bottom height may become smaller. Experimental work on nonrotating gravity currents by Rottman and Simpson [3] has shown that, in the early stages, the displacement of the front is linear in time, so that the speed is indeed constant. At later times, speeds begin to slow and the displacement curve obeys a power law of either $t^{2/3}$ if there is an interaction with the end of the tank, or $t^{1/5}$ if viscous effects dominate; the time and nature of such a transition depends on the Reynolds number of the current, though in all cases the viscous profile eventually dominates.

The formation and evolution of a gravity current under the effects of rotation has been studied extensively, and has been reviewed by Griffiths [4]. The classic geostrophic adjustment problem of Rossby [5] was extended to a rotating channel flow by Gill [6], who considered the adjustment of two semi-infinite channels filled with fluid of infinitesimally different heights and separated by a barrier. Using linearized dynamics, it was shown that, for a channel of width larger than, but still comparable to, the radius of deformation, the adjustment process is initially driven by the propagation of gravity waves, just as for a nonrotating fluid. But after an inertial period of $2\pi f^{-1}$, where f is the Coriolis parameter, a semigeostrophic balance is established and the adjustment process is then dominated by the propagation of coastal Kelvin waves away from the location of barrier release. Since these waves travel along the boundaries in opposite directions, with the coast to the right of the direction of propagation (for $f > 0$), they give rise to gravity currents that hug the coast in a similar manner. This analysis has been extended to the case of finite difference of fluid height in a number of later studies (e.g., [7, 8]). The result of Benjamin mentioned earlier was generalized to rotating currents by Stern, Whitehead, and Hua [9], who found that the speeds of these currents are also constant, but that, because certain quantities remain indeterminate without a more rigorous analysis, the estimate for c becomes an upper bound.

Although the dynamics of gravity currents, both in the absence and presence of rotation, are understood in some detail, there has been less focus on how they are influenced by double diffusion. Laboratory experiments have shown that, for fluids with compensating temperature and salinity gradients, double diffusive effects can induce intrusions into each fluid, in the form of interleaving patterns [10, 11]. The effect of shear on the magnitude of the interfacial density flux has also been considered [12]. But direct studies of double diffusive gravity currents are few. Maxworthy [13] provided the first thorough experimental study of such currents, focusing on two-layer experiments of both constant flux and constant volume. He considered currents whose layer density differences were on the order of 10^{-3} to 10^{-2} g cm $^{-3}$, many times larger than in the study presented here. At early times, these currents exhibited behavior common to strongly inertial nondiffusive currents, such as the formation of a bulbous head and a constant frontal propagation rate (i.e. head speed). The propagation rates also did not differ noticeably from nondiffusive currents of the same density difference. At later times however, the heads would narrow to sharp peaks and, in the case of a finger favorable current, strong convection would begin, carrying heavy fluid downward and leading to the formation of a second, bottom gravity current. The speeds would also drop dramatically at this stage, and in some cases would stop completely.

Yoshida, Nagashima, and Ma [14] approached this problem from a different perspective by noting that a double diffusive mass exchange across the interface should increase the layer density difference over time, and thereby accelerate the gravity currents in some way. They suggest that the layer density differences considered by Maxworthy were too large to notice such a change, and so they looked at the evolution of double diffusive gravity currents with density differences that were at least an order of magnitude smaller. They were able to demonstrate that the double diffusive currents are notably faster than the nondiffusive ones. But because of the indirect method used to specify the density of each layer, they were unable to make a direct comparison between, say, finger favorable and nondiffusive, but otherwise identical, currents. They also showed that the finger favorable currents produced

a secondary bottom current, similar to those observed by Maxworthy.

In this study we follow an approach similar to that of Yoshida et. al. by using density differences on the order of $10^{-4} \text{ g cm}^{-3}$, though we also reduce the fluid height. While this makes our currents more susceptible to frictional effects, the small initial density differences and low speeds also make them highly sensitive to double diffusive fluxes. In Section 2 we describe our laboratory setup and the experiments performed. Sections 3 and 4 contain our results for the propagation rate of the fronts and their lateral spread. Analysis of the results, with a focus on the small-scale structure, is provided in Section 5. Conclusions and suggested areas for future work are discussed in Section 6.

2 Experimental Setup

2.1 Apparatus

Two sets of lock-exchange gravity current experiments were performed at the Woods Hole Oceanographic Institution. Both used an acrylic tank of dimensions 60 cm long, 10 cm wide, and 20 cm high, with a barrier located at the center (30 cm) point. The first set of experiments were done for a nonrotating system, and the setup is denoted schematically on Figure 1. The second set utilized a rotating table, shown in Figure 2.

For each lock-exchange experiment, two solutions of different densities and concentrations were prepared, using salt and sugar as our fast and slow diffusers¹. The densities for each solution were specified by first adding the amount of solute prescribed by Ruddick and Shirtcliffe [15]. We then refined the density by dilution or addition of solute, based on measurements from an Anton Paar DMA58 density meter. This allowed us to attain the desired density within $10^{-5} \text{ g cm}^{-3}$. All solutions were prepared from storage vats of distilled water, which were given sufficient time to adjust to room temperature.

Each run required 500 ml of a designated “light” fluid of lower density and an equal amount of “heavy” fluid of higher density. Unless specified otherwise, the light fluid was dyed with blue food coloring, whose effect on density was taken into account. The fluids were poured into opposite ends of the tank, which were separated by a movable barrier. We then verified that the fluid heights on the two sides were equal, correcting each level if necessary. For the rotating cases, we allowed for 10 minutes of spinup time to let the system reach equilibrium. After the system settled, the barrier was then quickly but carefully removed, with as little disturbance to the fluid as possible, and the gravity current was allowed to develop.

2.2 Visualization

Two methods of visualization were used during these experiments. For observation of the vertical structure, a minimal amount of blue food color dye (less than 0.1 ml) was added to the lighter fluid to distinguish the individual fluid layers. A shadowgraph, illuminated by a projector light source, allowed for resolution of the small-scale double diffusive features. For the lateral structure of the rotating currents, 2 ml of food color dye was used to highlight the structure of the current profile. In both cases, images were collected with either a

¹The diffusivities of salt and sugar in water are 1.5×10^{-5} and $0.5 \times 10^{-5} \text{ cm}^2 \text{ sec}^{-1}$, respectively.

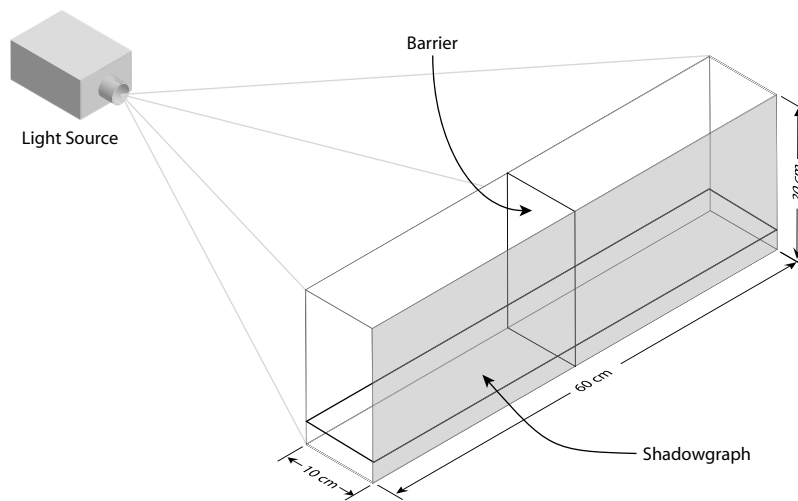


Figure 1: Experimental Setup for Nonrotating Experiments

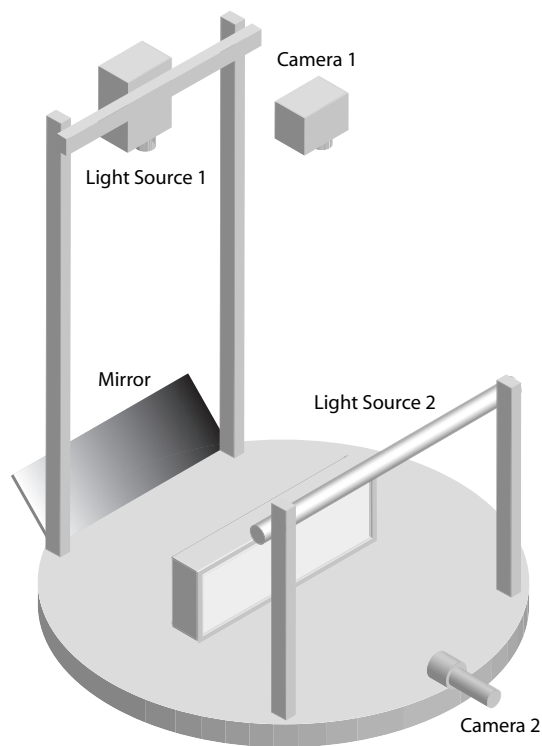


Figure 2: Experimental Setup for Rotating Experiments

black-and-white video camera for lower resolution video capture, or a digital still camera for higher resolution image analysis.

For most experiments, the overhead cameras track the propagation of the gravity current along the upper fluid surface. However, as mentioned before, currents with finger favorable profiles can produce secondary bottom currents that can, in more extreme cases, become the dominant gravity current and may tend to contain most of the dyed fluid. Our visualization methods will therefore track the bottom current in these situations. For such cases, it was confirmed that the top and bottom currents propagate at the same speeds however, so that for the purposes of speed comparison it is sufficient to track either current.

2.3 Experimental Parameters

Table 1 shows the physical parameters of the experiments to be discussed. The first row refers to the double diffusive process that one would expect from each experiment. For example, if we consider an experiment where light sugar water will flow above heavy salt water, then we would expect fingers to form. Such currents are referred to as finger favorable (hereafter FF) currents. Similarly, a flow with light salt water over heavy sugar water would be expected to form a diffusive layer, and the currents are said to be diffusive layer favorable (hereafter DF). We would not expect any significant diffusive behavior if both fluids contain only salt, or only sugar.

Table 1: Experimental Parameters

Parameter	Values
Double Diffusive Tendency	Fingers, Diffusive Layers, or Single Component
Rotation Rate (f)	0.0 or 1.0 rad sec ⁻¹
Prospective Difference ($\Delta\rho$)	5.0×10^{-4} or 1.2×10^{-4} g cm ⁻³
Mean Density (ρ)	1.02 or 1.04 g cm ⁻³
Fluid surface height (h)	1.7 cm

Table 2: Physical and dimensionless parameters ($U \approx 0.03\text{--}0.15$ cm sec⁻¹)

Parameter	$\Delta\rho = 0.0005$	$\Delta\rho = 0.00012$
$c = \sqrt{g'h}$	0.91 cm sec ⁻¹	0.44 cm sec ⁻¹
$L = c/f$	0.91 cm	0.44 cm
$Fr = U/c$	0.03–0.16	0.07–0.34
$Ro = U/fL$	0.03–0.16	0.07–0.34
$Re = Uh/\nu$	5.1–25.5	5.1–25.5

We also consider the effects of rotation, density difference between layers, and solute concentration of the fluids. We specify the rotation rate in terms of the Coriolis parameter, $f = 2\Omega$, where Ω is the true rotation rate of the table. The density difference between layers is established during preparation of the fluids, in the manner described before. The mean density is equivalent to solute concentration. The fluid height h results from the use

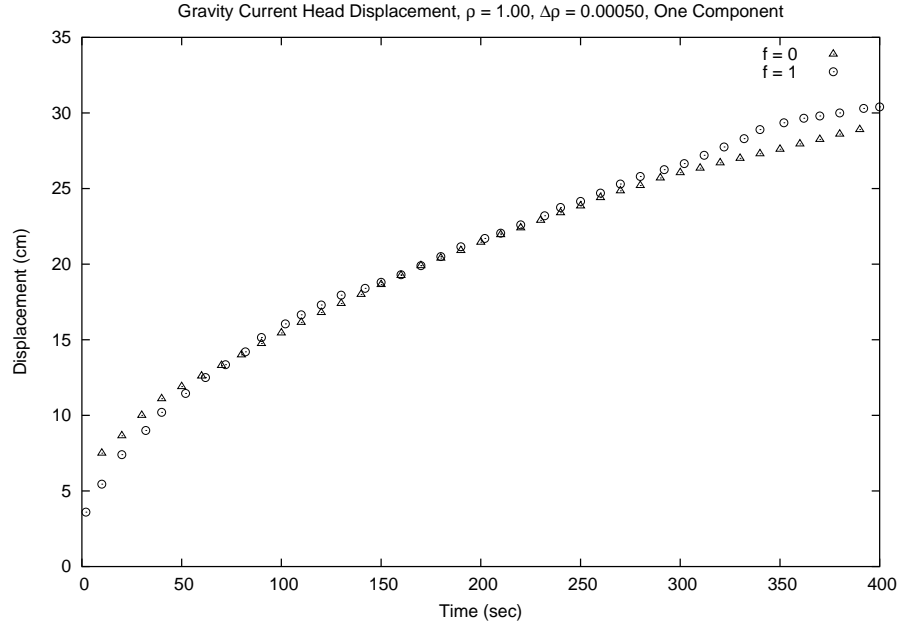


Figure 3: Effect of rotation on a nondiffusive current with a large $\Delta\rho$

of 1000 ml of fluid in our particular tank. A complete set of the experiments performed is shown in Tables 3 and 4, shown at the end of this manuscript.

Table 2 gives some estimates for the dynamical and dimensionless parameters of our experiments, based on empirical observations of gravity current head speeds of $0.03\text{--}0.15\text{ cm sec}^{-1}$. The dynamical parameters, c and L , are the estimates for the (shallow water) gravity wave speed and Rossby radius of deformation, respectively. The dimensionless parameters are estimates for the Froude, Rossby, and vertical Reynolds numbers of our experiments. We see that Froude and Rossby numbers are small, and so we should expect some sort of geostrophically or quasigeostrophically balanced flow, with rapid adjustment by the internal gravity waves. Reynolds numbers are, however, only modestly large, so we can only presume that viscous effects will play a significant role in the dynamics of the gravity currents.

3 Frontal Propagation

In this section we provide a quantitative description of the propagation rate of the interfacial front of a two layer double diffusive gravity current, and its variation in response to the following effects: rotation, double diffusive tendency, density difference between layers, and solute concentration.

3.1 Rotation

We first consider the response of a current to rotation. The head speed of a single component current with and without rotation is shown in Figure 3. The plot shows that there is close agreement between the two curves during the intermediate period of 50–200 sec, but there

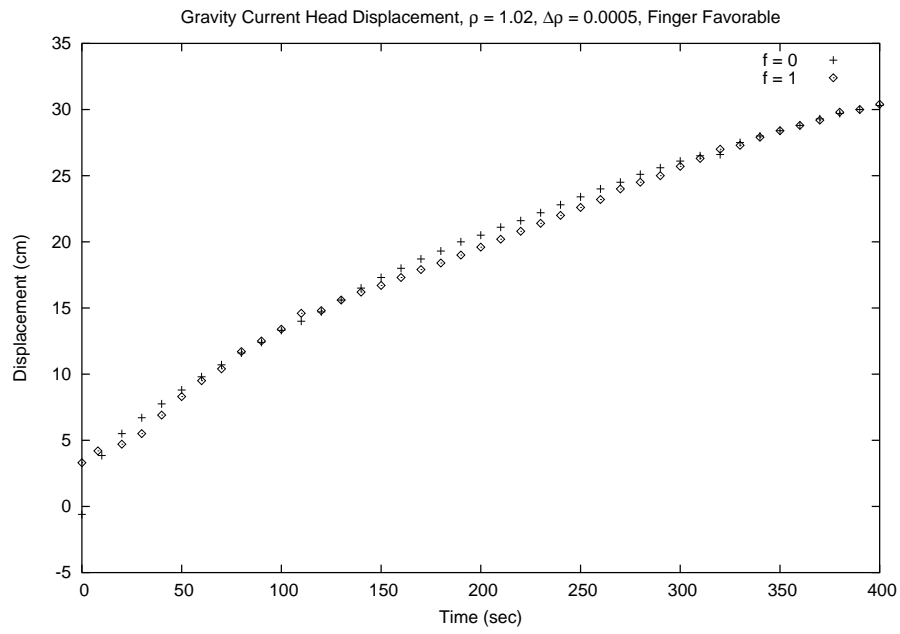


Figure 4: Same as Figure 3, for a FF current

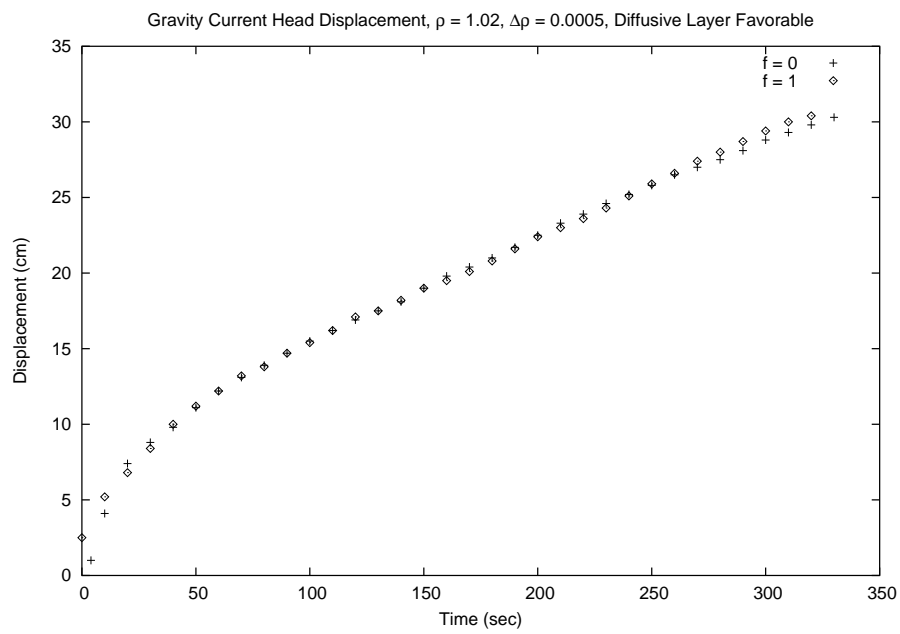


Figure 5: Same as Figure 3, for a DF current

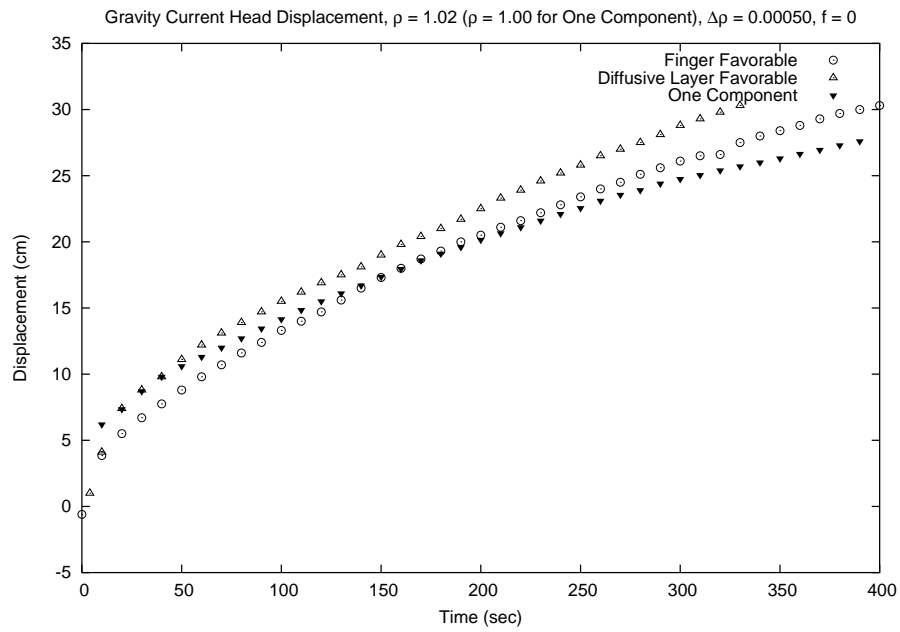


Figure 6: Effect of double diffusion on a nonrotating gravity current with large $\Delta\rho$

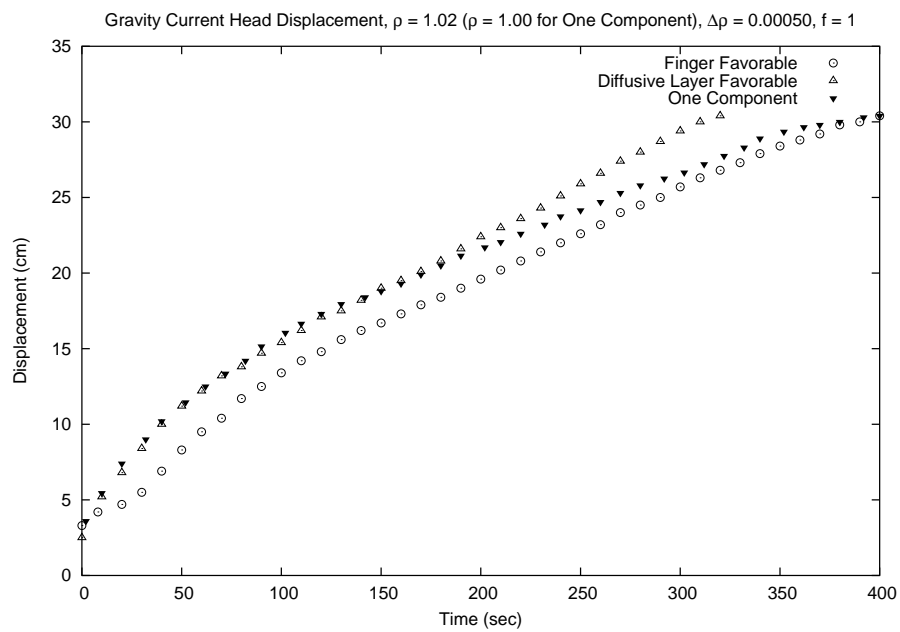


Figure 7: Same as Figure 6, with rotation

is a noticeable discrepancy at later times, particularly as the gravity current reaches the end of the tank.

Figure 4 shows that there is also close agreement between the rotating and nonrotating curves for the FF gravity currents. The agreement is even better between the DF currents, shown in Figure 5. In both cases, the curves appear to be piecewise linear, with transitions occurring after about one minute. This is somewhat expected, since frictionless currents have been shown to propagate at constant speeds [2, 9]. But it is surprising that this particular state would dominate for so long, since our Reynolds numbers are not very large and viscosity would be expected to have a substantial influence on the propagation, as shown by Rottman and Simpson [3].

In all three scenarios, we find that there is reasonable agreement between the head speeds of rotating and nonrotating gravity currents. This is an indication that the fluid velocities perpendicular to the current motion, and resulting Coriolis forces along the current, are small and have little effect on frontal propagation. Consequently, the dynamics along the current are largely inertial, with the acceleration driven by a lateral pressure gradient and modified by viscous forces. And since speeds are much larger in the direction of the current, the Coriolis forces are significant in the direction perpendicular to the current propagation and we would expect a crossflow geostrophic balance. This is demonstrated by the formation of a boundary current in all rotating cases, such as those in Figures 13–18.

3.2 Double Diffusive Tendency

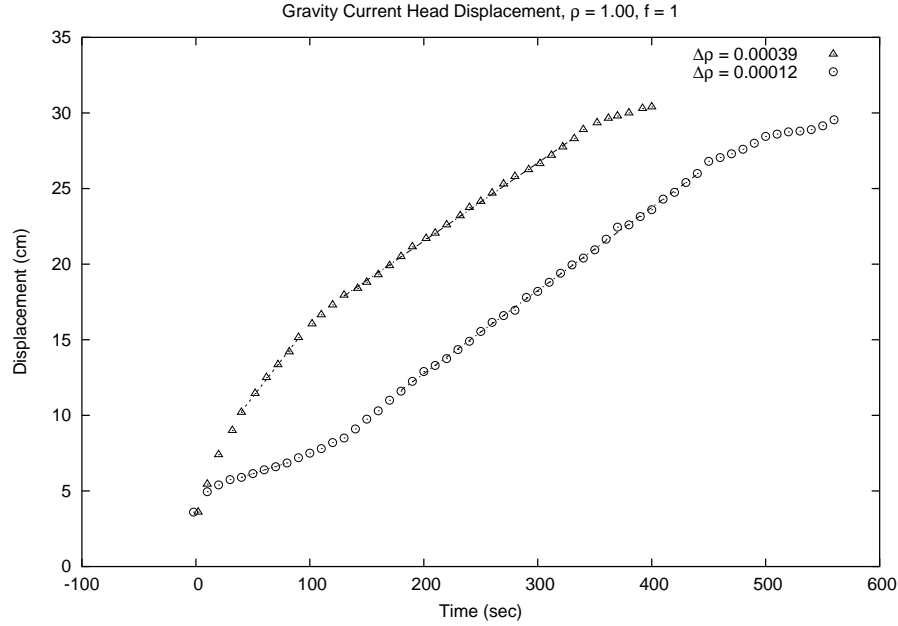
Figures 6 and 7 demonstrate, in the absence and presence of rotation, respectively, the behavior of gravity currents that have different double diffusive profiles but are otherwise equivalent. In both plots, the double diffusive gravity currents are significantly faster than the nondiffusive ones. For the rotating cases, there are intermediate regimes where the speed profile appears to be approximately linear.

If we focus on Figure 7 but appeal to the linear fits of the intermediate regimes of the same curves that appear in Figures 8, 9, and 10 (namely, the curves for large $\Delta\rho$ in each plot), then we see that the DF currents are 33% faster than the nondiffusive currents, while the FF currents are only about 13% faster. The greater speeds of the double diffusive currents are most likely a consequence of the increasing density difference between layers over time. This can in principle lead to a stronger acceleration and larger head speed.

3.3 Density Difference Between Layers

The most dramatic behavior in head speed is exhibited by variation of the initial density difference between layers. Hereafter, we will restrict our attention to data from rotating experiments. We also use curve fitting to estimate the head speeds for some of the observed linear regimes. While this method is somewhat subjective because it is not always clear where the linear regimes begin and end, it provides a quantitative estimate for comparative purposes.

Figures 8, 9, and 10 demonstrate two general responses to changes of initial layer density difference, the first being that the strong initial surge associated with large density differences is much weaker, if it occurs at all, when the density difference is reduced. The



$\Delta\rho$ (g cm^{-3})	U (cm sec^{-1})	Δt (sec)
0.00039	0.097	40–90
0.00039	0.052	130–330
0.00012	0.024	40–80
0.00012	0.055	180–440

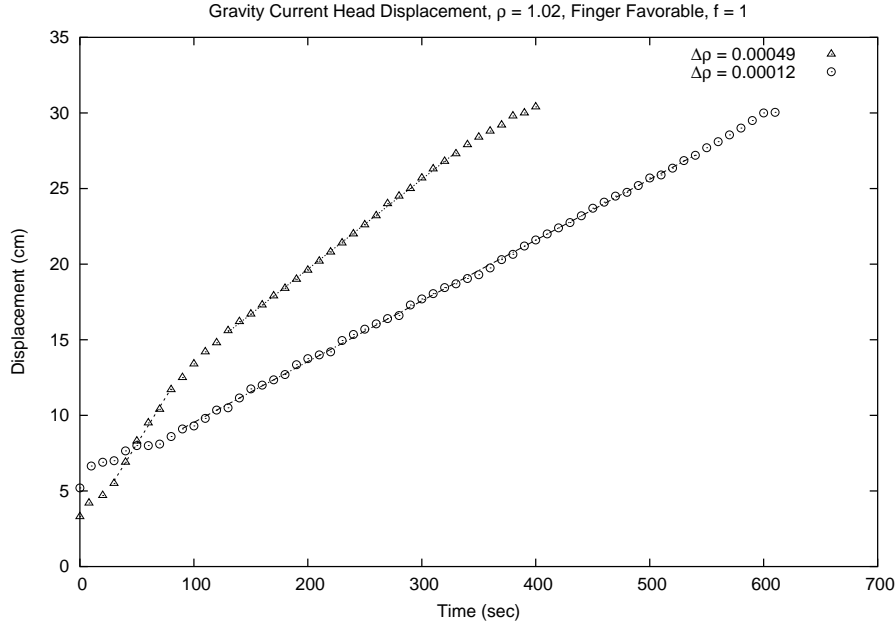
Figure 8: Effect of layer density difference on a nondiffusive current with rotation

second, more predictable, result is that head speeds become larger as density differences are increased.

Figure 8 illustrates a dramatic feature which is observed only in nondiffusive currents. We see that when the density difference is very small, the head speed is initially much less than the gravity current with a larger density difference. But after about two minutes, this slower current begins to separate from the wall and the speed increases dramatically. Evidence of this separation can be seen in Figure 16. The table corresponding to Figure 8 shows that the speeds of the currents in the two cases are in fact comparable. Some speedup after separation is expected, since there should be less viscous drag along the sidewall. But it is surprising that the speedup would be so dramatic, and that it would match the speed of the current with a larger density difference.

Such separation is not observed among the double diffusive currents. Figure 9 shows the evolution of FF gravity currents with large and small initial density differences. At early times (until about the first minute), the current with a large density difference is relatively fast, while the current of small difference appears to be much slower. At later times we have more predictable results, with the larger $\Delta\rho$ producing currents that are about 50% faster than the smaller $\Delta\rho$, as we see from the table below Figure 9.

Figure 10 and the corresponding table show that the DF currents exhibit some behavior



$\Delta\rho$ (g cm^{-3})	U (cm sec^{-1})	Δt (sec)
0.00049	0.122	30–80
0.00049	0.059	130–330
0.00012	0.040	90–540

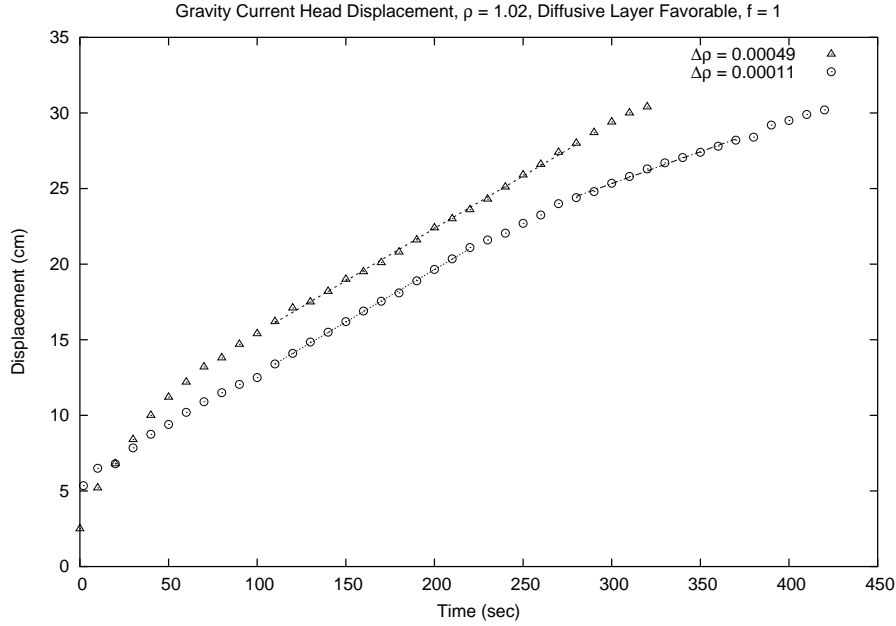
Figure 9: Effect of layer density difference on a FF current with rotation

that is similar to the FF case. However, there are some notable distinctions between the FF and DF currents when the density difference is small. After the first two minutes, this current's speed is nearly the same as the one with a large initial density difference. It is only after about five minutes that there is an abrupt reduction in speed, so that the current with a large difference is nearly 66% faster than the current with a small difference.

In both cases the currents have greater head speeds when the initial density differences are larger, but the speeds do not scale like $\sqrt{\Delta\rho}$, which one might expect from dimensional arguments or comparison to theoretical results [2, 9]. One possible reason for this is that the head speed is nonzero even when $\Delta\rho$ is initially zero, which has been demonstrated in previous studies [16], and is a consequence of increasing density difference over time.

3.4 Solute Concentration

Figure 11 and the corresponding table show that, after a two minute adjustment period, the FF current with a higher solute concentration is more than 50% faster than the current of lower concentration. Both currents also appear to undergo a transition at roughly the same time. The effect is similar for the DF current, shown in Figure 12, which appears to approach its dominant speed more rapidly, occurring after about a minute. The higher concentration current is also nearly 50% faster than the lower concentration one, and resembles



$\Delta\rho$ (g cm^{-3})	U (cm sec^{-1})	Δt (sec)
0.00049	0.069	110–280
0.00011	0.069	110–220
0.00011	0.042	280–370

Figure 10: Effect of layer density difference on a DF current with rotation

the behavior of the FF current.

Our results demonstrate that solute concentration can be as significant of a factor as the density difference when the density differences are very small. Just as a stronger concentration gradient will typically drive a greater diffusive flux, in a Fickian sense, it is not surprising that double diffusive fluxes across the interface will also be intensified in the presence of stronger solute gradients.

4 Current Structure

We now focus on the lateral structure of the currents. In all cases where rotation is involved, coastal currents are formed, shown in Figures 13, 14, and 15 for a density difference of approximately $5 \times 10^{-4} \text{ g cm}^{-3}$. The most distinguishing feature of the double diffusive currents (shown in Figures 14 and 15) is that the shear-like protrusions associated with the nondiffusive fronts are no longer present. Such protrusions were first studied by Stern [17], and a more recent investigation has been conducted by Stern and Chassignet [18]. While the diffusive currents often exhibit a wavy interface, there is no sign of the sharp crests observed in the nondiffusive current. There is also a noticeable lateral spread, resulting in a broadening of the double diffusive currents as compared to the nondiffusive ones.

This spread is even more pronounced for currents where the density difference has been

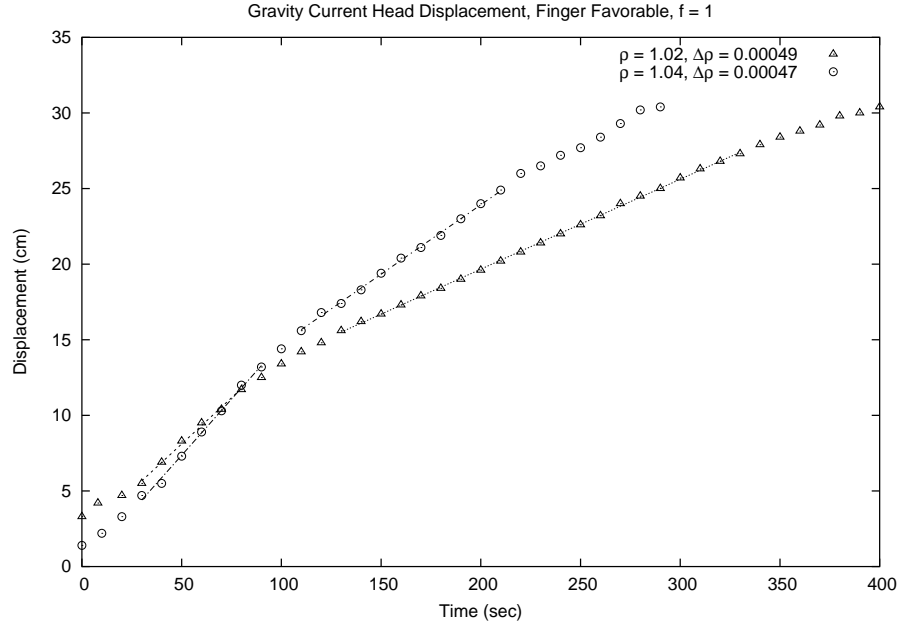


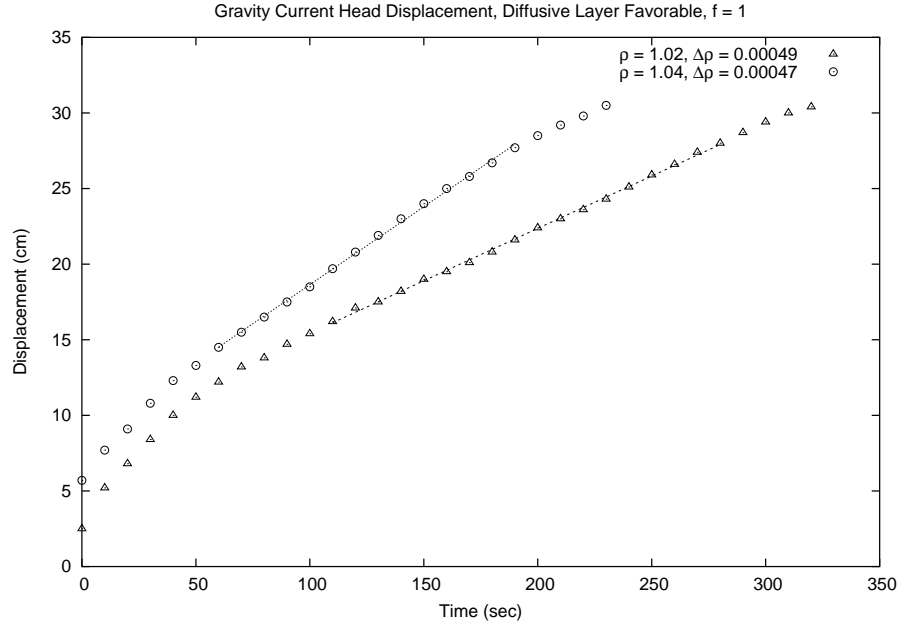
Figure 11: Effect of solute concentration on head speed of a FF current

reduced by a factor of four, shown in Figures 16, 17, and 18. It also appears that these currents tend to retain any vorticity that forms during barrier release for a much longer time; this is most evident in Figure 17. And as discussed earlier, the nondiffusive currents with small density difference tend to separate from the wall, observable in Figure 16. This is not seen in the double diffusive currents, and may be a consequence of the lateral spread. In any case, it is clear that double diffusive fluxes, and the changing density difference with time, are responsible for these differences.

5 Internal Flow Structure

Without an accurate means of measuring the density field over time, it is difficult to diagnose the influence of double diffusion on the gravity currents with great confidence. Nonetheless, observations provide clues about the flow structure and the dynamical processes behind them.

We first consider the flow of a DF current. From shadowgraph observations, we observe that, for a gravity current propagating to the right, there is a strong clockwise shear in the vicinity of the diffusive layer, with weaker counterclockwise shears within each layer. A vertical cross section showing the flow profile is given in Figure 19, and photographs



ρ (g cm^{-3})	U (cm sec^{-1})	Δt (sec)
1.02	0.069	110–280
1.04	0.103	60–190

Figure 12: Effect of solute concentration on head speed of a DF current

of a typical current are shown in Figure 22. We expect that diffusive transport across the layer will carry salt downward, making the fluid just above the layer lighter and the fluid just below it heavier. If the rate of diffusive transport is reasonably slow, then we would not expect an onset of convective mixing but instead an organized, buoyantly induced upward transport of lighter fluid along the interfacial slope in the top layer, and a downward transport of heavier fluid in the bottom layer. The increased flow rate would then lead to a greater gravity current speed. In general though, this induced flow will probably be greater than the increased frontal propagation rate, so that the current will reverse direction near the front. This would result in the counterclockwise shear flows within each layer, though the lower layer shear would be significantly reduced by bottom friction. Such shears would also be expected to induce mixing within each layer.

The evolution of a gravity current under a FF stratification is markedly different. The initial protrusion of the gravity current is illustrated in Figure 20. There should be an initial period of finger formation along the front, with freshened salt water moving upward and a salt-sugar mix moving downward. After these fingers penetrate deeply into each layer, they will eventually become unstable and induce local convective mixing near the top and bottom of the fluid. This will eventually lead to the creation of a very fresh solution atop, with the original sugar and salt solutions inbetween, and a very heavy salt-sugar solution at the bottom, shown schematically in Figure 21. The actual flow will not have the clear boundaries shown in this figure; the density variation will be more continuous



Figure 13: View from above of a rotating, nondiffusive gravity current, four minutes after release of the barrier; each tick on the scale represents one centimeter



Figure 14: Same as Figure 13, for a FF current



Figure 15: Same as Figure 13, for a DF current



Figure 16: View from above of a rotating, nondiffusive gravity current, four and a half minutes after release of the barrier.



Figure 17: Same as Figure 16, for a FF current



Figure 18: Same as Figure 16, for a DF current

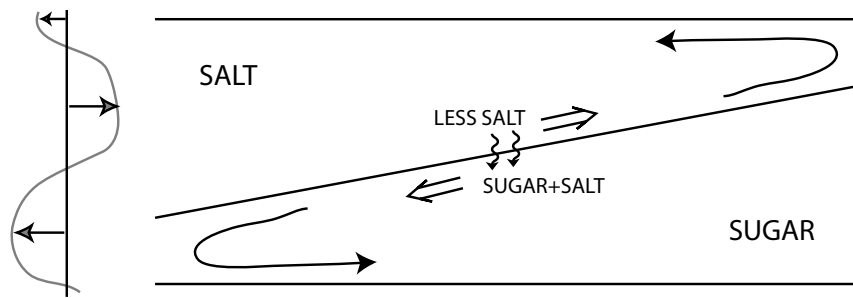


Figure 19: Flow structure of a DF current

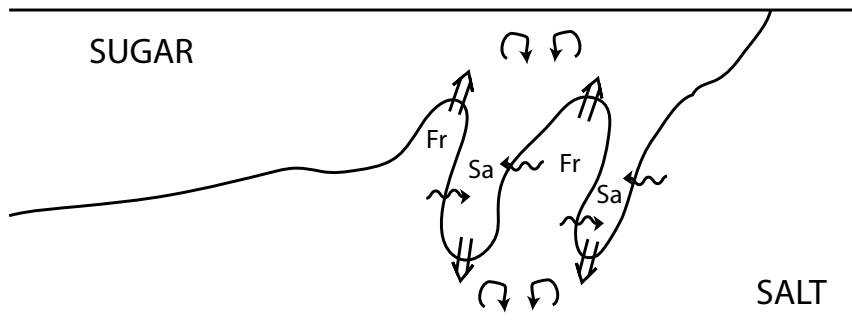


Figure 20: Early intrusion of a FF current

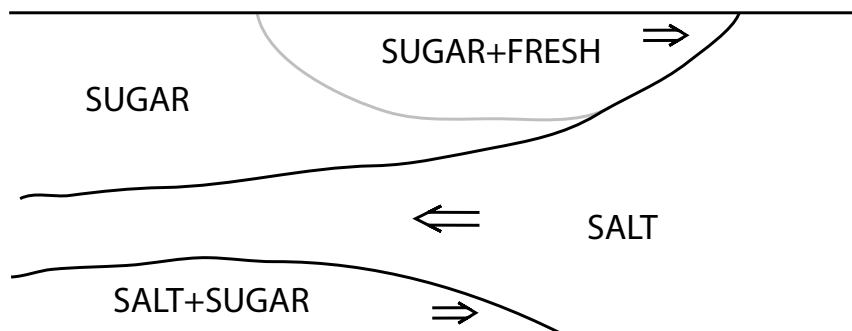


Figure 21: Schematic of a FF current after induced mixing

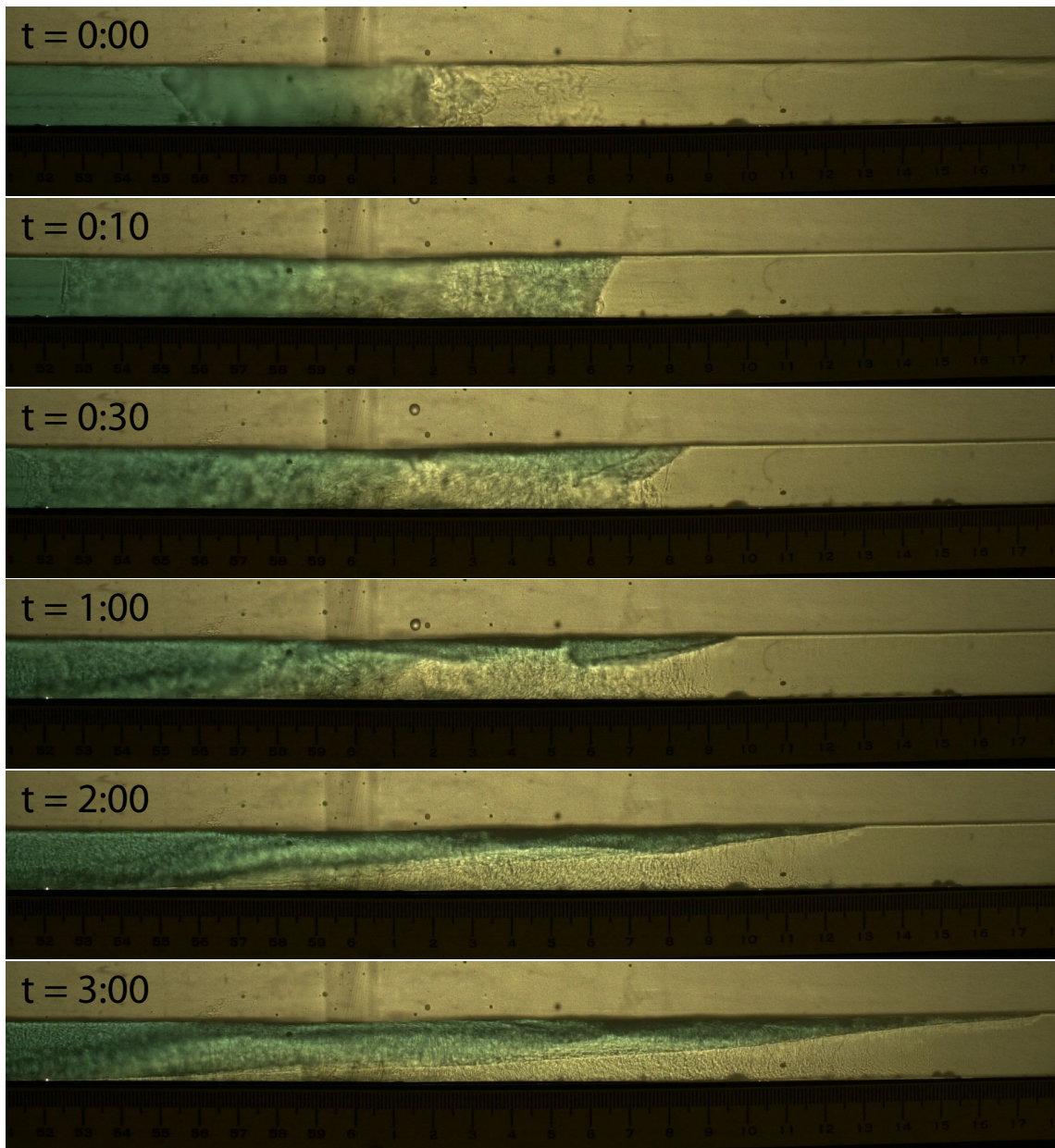


Figure 22: Evolution of a DF gravity current

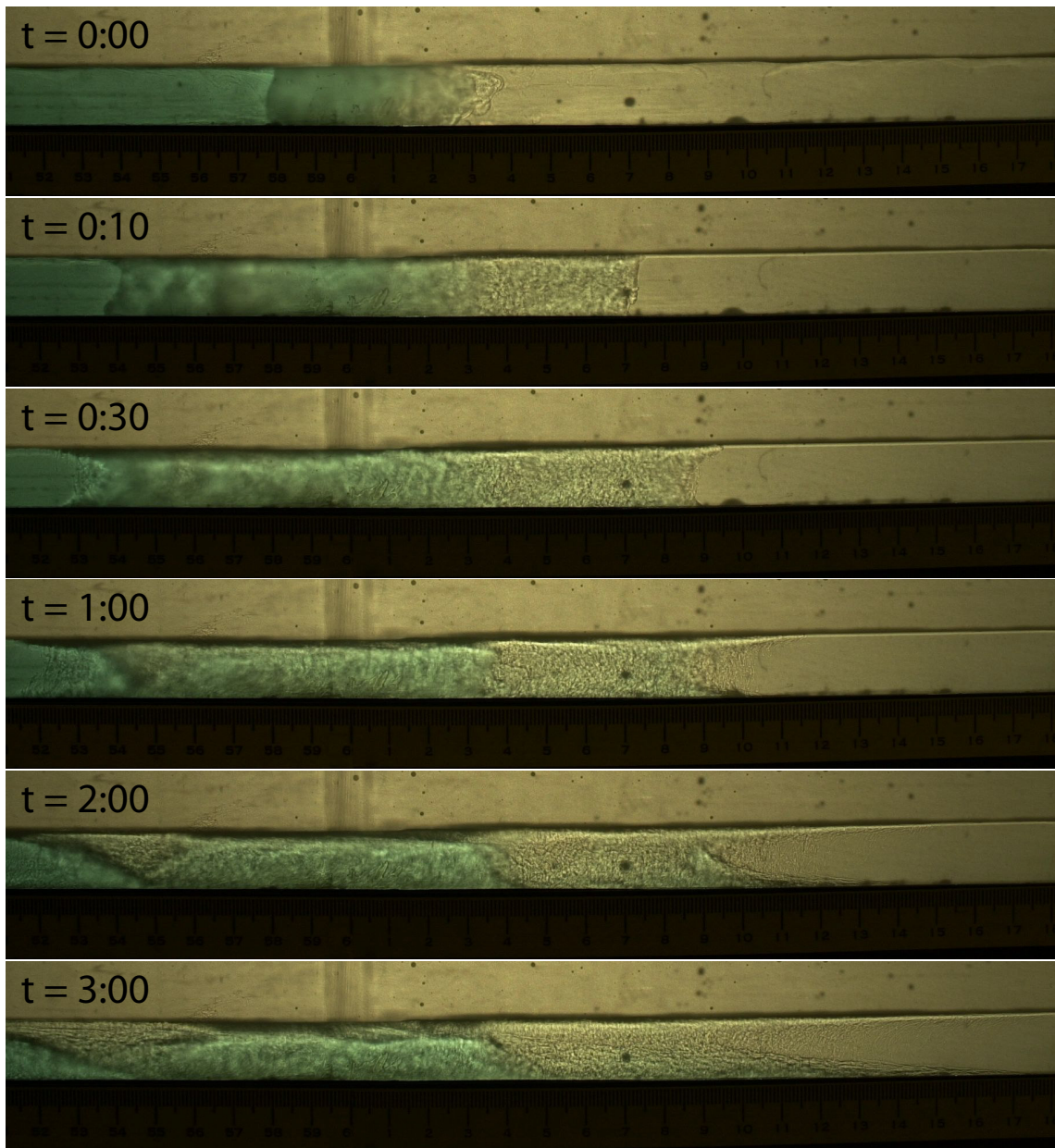


Figure 23: Evolution of a FF gravity current

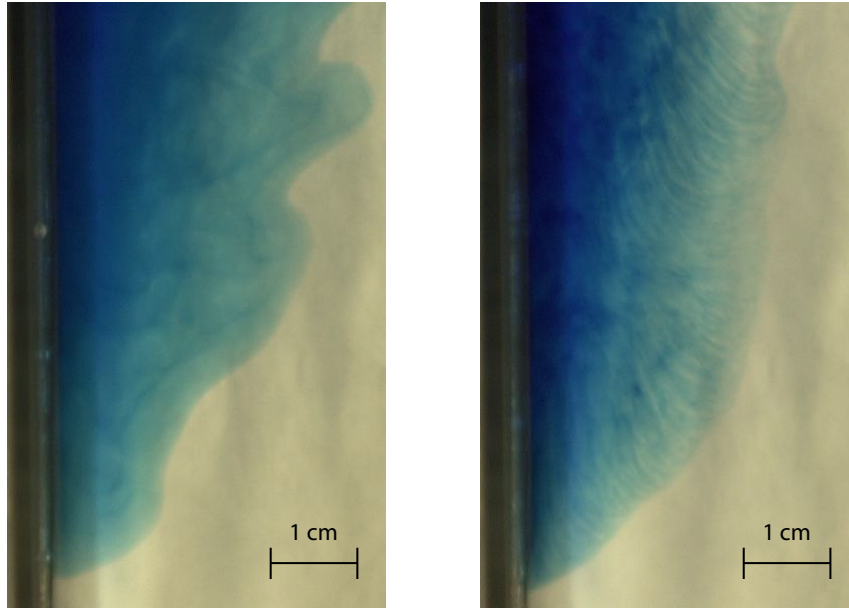


Figure 24: Topview profiles of rotating DF (left) and FF (right) gravity currents with a large density difference and small concentration

and the regions will not be as well-defined in the presence of convective mixing. But after the fluid settles, this activity would result in the formation of two gravity currents, both a very light current atop and a heavy current along the bottom, as reported in prior experimental studies [13, 14], and is most pronounced when the density differences are very small and solute concentration is large. Photographs illustrating this process are shown in Figure 23. In such cases, the top current is nearly invisible and the bottom current is the dominant structure, making it appear that the light and heavy fluids have switched roles. The bottom current is presumably DF, while the top may be weakly FF. Figure 24 clearly shows the presence of fingers atop of a FF current with large density difference and small concentration, supporting this hypothesis.

6 Conclusions and Future Work

In this study we have attempted to determine the role of double diffusion and rotation on gravity currents by examining their response to various double diffusive profiles, initial density differences, and solute concentrations. Double diffusive currents exhibited a greater head speed than nondiffusive currents that were otherwise identical, with the DF currents being faster than the FF currents, which is consistent with previous studies. We also find that head speeds increase when the density difference and solute concentration between layers become greater. The head speed is therefore much more complicated than for a nondiffusive current; very large density differences in previous studies that were at least an order of magnitude greater than in the present study produced currents that scaled like $\sqrt{\Delta\rho}$, while for the currents presented here, $\Delta\rho$ is clearly increasing with time and the speed

does not scale simply like the initial density difference. This fact, along with the increased sensitivity to concentration, suggest that double diffusive fluxes can play a significant role in frontal propagation of gravity currents. In any case, the head speeds are observed to be independent of rotation, regardless of the relative importance of double diffusion.

Rotation has the greatest effect on the lateral structure of these currents. Boundary currents form in all rotating cases, but the structure is greatly modified by double diffusion. The shear-like crests associated with the nondiffusive rotating currents are no longer present when the density profiles are double diffusive. Wall separation, which seems to be associated with very small density differences in nondiffusive currents, does not seem to occur. In addition, the crossflow spread is much greater when double diffusion is introduced. This spreading, undoubtedly due to the double diffusive fluxes and associated increase of $\Delta\rho$, may very well be responsible for the reduction of frontal instabilities and lack of wall separation.

To better understand the dynamics behind propagation of the fronts and their lateral structure, especially concerning the formation of instabilities and rate of spread, a robust scale analysis that incorporates the density difference and solute concentration into the double diffusive flux is required. Further experiments should also be conducted to establish the sensitivity of the currents to these parameters. Finally, the role of viscosity must be resolved. A simple theoretical treatment of certain idealized flows would help greatly in all of these efforts.

7 Acknowledgements

This project would not have been possible without George Veronis, who not only suggested the topic but also provided continuous guidance in both the laboratory and the subsequent discussions. I will always remember our many conversations together, and I may have even learned to enjoy softball. I am also grateful to Keith Bradley for his time and effort in setting up the more elaborate parts of the experiments, and teaching me how to do the rest. I also want to acknowledge helpful discussions with Karl Helfrich and Jack Whitehead. Finally, I want to thank all of the GFD summer program staff and other fellows for providing me with an incredible educational opportunity and happy memories of my time here.

References

- [1] J. J. Stoker, *Water Waves* (Interscience, New York, 1957).
- [2] T. B. Benjamin, "Gravity currents and related phenomena," *J. Fluid Mech.* **31**, 209 (1968).
- [3] J. W. Rottman and J. E. Simpson, "Gravity currents produced by instantaneous releases of a heavy fluid in a rectangular channel," *J. Fluid Mech.* **135**, 95 (1983).
- [4] R. W. Griffiths, "Gravity currents in rotating systems," *Ann. Rev. Fluid Mech.* **18**, 59 (1986).
- [5] C. G. Rossby, "On the mutual adjustment of pressure and velocity distributions in certain simple current systems," *J. Mar. Res.* **1**, 19 (1937).

- [6] A. E. Gill, “Adjustment under gravity in a rotating channel,” *J. Fluid Mech.* **77**, 603 (1976).
- [7] A. J. Hermann, P. Rhines, and E. R. Johnson, “Nonlinear Rossby adjustment in a channel: beyond Kelvin waves,” *J. Fluid Mech.* **205**, 469 (1989).
- [8] K. R. Helfrich, A. C. Kuo, and L. J. Pratt, “Nonlinear Rossby adjustment in a channel,” *J. Fluid Mech.* **390**, 187 (1999).
- [9] M. E. Stern, J. A. Whitehead, and B.-L. Hua, “The intrusion of a density current along the coast of a rotating fluid,” *J. Fluid Mech.* **123**, 237 (1982).
- [10] J. S. Turner, “Double-diffusive intrusions into a density gradient,” *J. Geophys. Res.* **83**, 2887 (1978).
- [11] B. R. Ruddick and J. S. Turner, “The vertical length scale of double-diffusive intrusions,” *Deep-Sea Res.* **26**, 903 (1979).
- [12] P. E. Linden, “Salt fingers in steady flow,” *Geophys. Fluid Dyn.* **6**, 1 (1974).
- [13] T. Maxworthy, “The dynamics of double-diffusive gravity currents,” *J. Fluid Mech.* **128**, 259 (1983).
- [14] J. Yoshida, H. Nagashima, and W. Ma, “A double diffusive lock-exchange flow with small density difference,” *Fluid Dyn. Res.* **2**, 205 (1987).
- [15] B. R. Ruddick and T. G. L. Shirtcliffe, “Data for double diffusers: Physical properties of aqueous salt-sugar solutions,” *Deep-Sea Res.* **26A**, 775 (1979).
- [16] A. F. Thompson, in *Proceedings of the 2003 Summer Study Program in Geophysical Fluid Dynamics* (Woods Hole Oceanographic Institution, Woods Hole, MA, 2003), pp. 146–165.
- [17] M. E. Stern, “Geostrophic fronts, bores, breaking and blocking waves,” *J. Fluid Mech.* **99**, 687 (1980).
- [18] M. E. Stern and E. P. Chassignet, “Mechanism of eddy separation from coastal currents,” *J. Mar. Res.* **58**, 269 (2000).

Experiment	Diffusive Tendency	Density Difference	Mean Density
1	Diffusive Layer	0.00046	1.02
2	Diffusive Layer	0.00044	1.02
5	Fingers	0.00046	1.02
6	Nondiffusive	0.00048	1.00
7	Diffusive Layer	0.00053	1.02
8	Fingers	0.00051	1.02
9	Fingers	0.00048	1.02
10	Diffusive Layer	0.00050	1.02
11	Diffusive Layer	0.00011	1.02
12	Diffusive Layer	0.00013	1.04
13	Diffusive Layer	0.00012	1.02
14	Fingers	0.00012	1.04
15	Fingers	0.00014	1.04
16	Fingers	0.00012	1.04
17	Diffusive Layer	0.00013	1.04
53	Fingers	0.00050	1.02
54	Diffusive Layer	0.00050	1.02

Table 3: Table of nonrotating experiments. Experiments 3 and 4 were removed because of operational error.

Experiment	Diffusive Tendency	Density Difference	Mean Density
18	Nondiffusive	0.00049	1.00
19	Fingers	0.00047	1.02
20	Fingers	0.00049	1.02
21	Diffusive Layer	0.00051	1.02
22	Diffusive Layer	0.00046	1.02
23	Fingers	0.00015	1.02
24	Diffusive Layer	0.00002	1.02
25	Diffusive Layer	0.00012	1.02
26	Nondiffusive	0.00010	1.00
27	Diffusive Layer	0.00013	1.02
28	Nondiffusive	0.00050	1.00
29	Diffusive Layer	0.00049	1.02
30	Fingers	0.00049	1.02
31	Nondiffusive	0.00050	1.00
32	Fingers	0.00012	1.04
33	Fingers	0.00012	1.04
34	Diffusive Layer	0.00011	1.04
35	Diffusive Layer	0.00013	1.04
36	Fingers	0.00049	1.02
37	Diffusive Layer	0.00049	1.02
38	Fingers	0.00060	1.04
39	Diffusive Layer	0.00051	1.04
40	Fingers	0.00014	1.04
41	Fingers	0.00011	1.04
42	Diffusive Layer	0.00011	1.04
43	Nondiffusive	0.00039	1.00
44	Nondiffusive	0.00012	1.00
45	Fingers	0.00011	1.04
46	Diffusive Layer	0.00012	1.04
47	Fingers	0.00047	1.04
48	Diffusive Layer	0.00047	1.04
49	Fingers	0.00012	1.02
50	Diffusive Layer	0.00011	1.02
51	Fingers	0.00053	1.02
52	Diffusive Layer	0.00056	1.02

Table 4: Table of rotating experiments. Note that Experiment 24 is only diffusive layer favorable in a marginal sense, since the density difference is so small.